The Monte Carlo Independent Column Approximation: An Assessment using Several Global Atmospheric Models

H. W. Barker[1], *J. N. S. Cole*[2], *J.-J. Morcrette*[3], *R. Pincus*[4], *P. Räisänen*[5], *K. von Salzen*[6], and *P. A. Vaillancourt*[7]

[1] Environment Canada, Toronto, ON, Canada

[2] University of British Columbia, Vancouver, BC, Canada

[3] European Centre for Medium-Range Weather Forecasts, Reading, Berkshire, UK

[4] NOAA-CIRES Climate Diagnostics Center, Boulder, CO, USA

[5] Finnish Meteorological Institute, Helsinki, Finland

[6] Environment Canada, Victoria, BC, Canada

[7] Environment Canada, Montreal, QC, Canada

Submitted to: *Q. J. R. Meteorol. Soc.,* Mar. 17, 2008

revised: July 2, 2008

---

* *Corresponding author address*: Howard Barker, Environment Canada, Cloud Physics and Severe Weather Research Section (ARMP), 4905 Dufferin St., Toronto, ON, Canada M3H 5T4. E-mail: howard.barker@ec.gc.ca

Abstract

The Monte Carlo Independent Column Approximation (McICA) computes domain-average, broadband radiative flux profiles within conventional global climate models (GCMs). While McICA is unbiased with respect to the full ICA, it generates, as a by-product, random noise. If this by-product affects statistically significant impacts on GCM simulations, it could limit the usefulness of McICA. This paper assesses the impact of McICA's random noise on six GCMs. To this end, the GCMs performed ensembles of 14-day long simulations for various renditions of McICA; each with differing amounts of random noise. As seen in the past, low cloud fraction and surface temperature were affected most by noise. However, all GCM simulations using operationally viable renditions of McICA showed no statistically significant impacts; even for precipitation, a highly intermittent variable that one might expect to be sensitive to random fluctuations. Two GCMs showed statistically significant responses using an *academic* version of McICA that generates overly large sampling noise. Time series analyses of high resolution (i.e., typically 2 hourly) data revealed that fluctuations associated with most variables and GCMs are immune to McICA noise. Moreover, the nature of these fluctuations can vary substantially among GCMs and most often they overwhelm any noise impacts. Overall, the results presented here corroborate a range of previous studies done on one GCM at a time: random noise produced by recommended versions of McICA has statistically insignificant affects on GCM simulations.

1 Introduction

1.1 Background

It is recognized widely that if general circulation models (GCMs) are to satisfactorily simulate Earth's climate, physical processes responsible for hydro-radiative feedback mechanisms must be addressed and represented well (e.g., Aires and Rossow 2003; Randall et al. 2003). Failing to cross this ill-defined line, a GCM stands a good chance of serving only to heighten confusion surrounding explanation, and thus simulation, of the Earth-atmosphere system (cf. IPCC 2007). Central to adequate representation of hydro-radiative feedbacks lies numerical simulation of atmospheric radiative transfer (e.g., Stephens 2005).

The common purpose for doing radiative transfer calculations in GCMs is to provide atmospheric and surface broadband flux convergence rates. Since the mid-1970s GCMs have employed multi-layer two-stream approximations (TSAs) of the radiative transfer equation (RTE) (Meador and Weaver 1980). At the heart of TSAs is the assumption that atmospheric layers are horizontally homogeneous. Hence, radiation flowing within a GCM column is assumed not to interact with neighbouring columns. This is the independent column approximation (ICA) (Stephens et al. 1991). Given that horizontal grid-spacings exceed 50 km in most GCMs, it is reasonable to apply the ICA at a GCM's inner-scale.

Given the task at hand, multi-layer TSA algorithms eventually came to address columns whose layers were only partially filled by clouds which, in turn, overlapped vertically according to idealized rules; notably maximum-random overlap (MRO) (Geleyn and Hollingsworth 1979; Morcrette and Fouquart 1986; Tian and Curry 1989; Stubenrauch et al. 1997). Given

that MRO systematically underestimates vertically-projected cloud fraction (Räisänen et al. 2004), GCM radiative transfer codes based on MRO *rely* on horizontally homogenous clouds that are too attenuative relative to variable clouds with the same mean optical thickness (cf. Barker et al. 1999, 2003; Cole et al. 2005).

While several attempts have been made to account for effects of horizontal variations in single-layer clouds (e.g., Stephens 1988; Davis et al. 1990; Cahalan et al. 1994; Barker 1996; Cairns et al. 2000), they resemble each other in that they use the TSA, strive for analytic expressions for layer reflectance and transmittance, but pay little attention to covariations in the horizontal and vertical. Oreopoulos and Barker (1999) recognized the untenability of investing the MRO scheme with horizontally variable clouds, but their model and results resembled other attempts to account for unresolved cloud fluctuations in 1D codes: limited ranges of applicability and, seemingly, irreconcilable biases relative to the ICA.

Judging from GCM radiative transfer algorithms developed from the late 1970s to early 2000s, it could be argued that a paradigm was established based on the logic:

> because radiative fluxes depend on cloud structure, this implies that descriptions of cloud structure at scales $\Delta x < \Delta x_{\mathrm{GCM}}$, where Δx_{GCM} is GCM grid-spacing, should be a subset of (i.e., built directly into) the radiative transfer algorithm.

There is, however, no sound reason to believe that this logic will lead to algorithms that either allow for satisfactory description of cloud properties or account properly for interactions between radiation and clouds at scales smaller than Δx_{GCM}. Indeed, models based on this logic seem bound to approximations, limitations, and biases.

1.2 The Monte Carlo-based solution

If a GCM's column were to be resolved into J subcolumns, and the ICA applied to them, domain-average, broadband fluxes would be defined as

$$\langle F \rangle = \frac{1}{J} \sum_{j=1}^{J} \sum_{k=1}^{K} F(j,k), \tag{1}$$

where K is the number of spectral intervals, and F is flux from a 1D solution of the RTE. While (1) is the standard aspired to by GCM radiation algorithms (Collins 2001), it is computationally intractable. As an alternative to (1), and the aforementioned 1D solvers, Barker et al. (2002) proposed the Monte Carlo ICA (McICA) method. McICA rests on sampling stochastically-generated subcolumns of a GCM column, performing 1D radiative transfer calculations on them, and averaging the results (Pincus et al. 2003, 2006; Räisänen et al. 2004). As sampling is done during spectral integration, McICA reduces (1) to a single sum over k.

McICA represents a distinct departure from conventional methods because it separates the description of unresolved media from the radiative transfer algorithm while remaining unbiased with respect to (1). As such, it is extremely flexible for it admits any one-point statistical description of unresolved media, and subgrid variability can be handled easily by any 1D solution of the RTE and not just TSAs. Moreover, because a basic TSA (e.g., Wiscombe 1977) is used, McICA execution times are close to, if not less than, those of conventional schemes. As a by-product, however, McICA produces flux profiles that contain sampling noise.

Three studies (Pincus et al. 2006; Räisänen et al. 2005; Morcrette et al. 2008) suggest

that McICA noise can be reduced to the point of having negligible impact on GCM simulations. Räisänen et al.'s (2005) tests with the National Center for Atmospheric Research (NCAR) Community Atmospheric Model version 1.8 (CAM-v1.8) showed, however, that if large enough, McICA's noise can have statistically significant affects on GCM simulations. Thus, the main point of the current study is to assess the sensitivities of several GCMs, with differing physical parametrizations and dynamical cores, to stochastic noise generated by McICA. To this end, each GCM, with various renditions of McICA and a suitable stochastic subgrid-scale cloud generator, performed 14-day ensemble simulations.

The following two sections describe the experiments and the GCMs involved in the intercomparison. The fourth section presents the magnitudes of McICA noise and summarizes the results of the experiments, and the final section contains conclusions.

2 Experimental design

Table 1 summarizes the GCMs used in this study. The experiments performed by each GCM follow those performed by Räisänen et al. (2005). These experiments are summarized in the following subsections, but first the rationale for the experiments is discussed.

2.1 Rationale

Stochastic fluctuations of radiative fluxes generated by McICA can be thought of as extraneous information injected into a GCM at its radiative timestep and grid-spacing. For a fairly noisy version of McICA, Räisänen and Barker (2004) estimated typical standard devi-

ations for instantaneous net surface irradiances to be $\sim$50 W m^{-2}; the vast majority due to solar radiation. From timestep-to-timestep and cell-to-cell, McICA noise is uncorrelated so standard deviations of accumulated fluxes decay like $1/\sqrt{N}$ where N is number of timesteps or gridpoints. Given that the radiative timestep for most GCMs is $\sim$1 h, the magnitude of McICA noise for diurnal-mean net surface fluxes is O(10 W m^{-2}). As can be seen in Fig. 1, this is much smaller than diurnal standard deviations for surface irradiance that arise via the diurnal solar cycle (which are approximately half the values shown). It stands to reason, therefore, that for McICA's noise to excite change, it would have to do so quickly. Likewise, if noise-induced, short-term impacts yield significant biases, one can expect those biases to effectively force slower climatic variables and thus jeopardize McICA's utility.

Following this line of reasoning, relatively short simulations should suffice to elucidate impacts of McICA's stochastic noise on *fast* components of the climate system. Since *slower* components, such as deep soil moisture and mixed-layer ocean temperature, respond to surface energy budgets integrated over weeks, it is hypothesized that if fast components do not respond to high frequency noise, long-term climate simulations will not respond either. This rationale resembles that of the U.S. DoE's Climate Change Prediction Program (CCPP) and Atmospheric Radiation Measurement (ARM) Program (CCPP-ARM) Parameterization Testbed (CAPT) study (Philips et al. 2004).

2.2 The experiments

Based on the reasoning just explained, 14-day long GCM simulations were used for this intercomparison. McICA fluctuations for surface fluxes integrated over two weeks are about

20 times smaller than instantaneous values. Following Räisänen et al.'s (2004) calculations, this corresponds roughly to radiative fluctuations associated with fortnightly mean total cloud fraction changes of $\sim$0.02. Hence, we are satisfied that if significant differences do not appear after 14 days, it is unlike that the noise could somehow tunnel-up at longer scales and significantly alter a simulation relative to a noiseless reference.

There are several versions of McICA that yield substantially different amounts of noise (see Räisänen and Barker 2004). The least noisy incarnation was defined as the reference. Most GCMs performed five experiments with varying amounts of noise, each consisting of a 10-member ensemble. The experiments are described in the following subsections. Ensembles were created for each experiment by starting the GCM 6 hours apart off a "spun-up" simulation. As such, the j^{th} ensemble member of all experiments had the same initial conditions. This initialization process is illustrated in Fig. 2.

Two sets of experiments were performed: one started from January 1, the other from July 1. This was to explore whether the impact of McICA stochastic noise is state-dependent in addition to GCM-dependent. All indications suggest that this is not the case so only January results are shown and discussed. In all cases, sea-surface temperatures were prescribed. For brevity, the following explanation of experiments assumes a radiation code based on the correlated k-distribution (CKD) method (Fu and Liou 1992); which was not always the case.

2.2.1 Experiment 1: 1COL

If a *single* subcolumn is generated stochastically at each timestep and spectral integration (over K quadrature points) is performed on that subcolumn, (1) becomes

$$\langle F \rangle = \sum_{k=1}^{K} F(\alpha, k) \tag{2}$$

where α represents *the* generated subcolumn. This approach yields copious McICA noise and is referred to as "1COL ". Moreover, it resembles the method used in the Goddard Institute for Space Studies GCM (per. comm., A. A. Lacis 2007).

2.2.2 Experiment 2: BASIC

Sampling is improved over 1COL by generating a subcolumn (cloudy or clear) for each integration point and computing flux as

$$\langle F \rangle = \sum_{k=1}^{K} F(\alpha_k, k) \tag{3}$$

where α_k represents one of K generated columns. Being the most straightforward, code-friendly version of McICA, it is referred to as the "BASIC "experiment.

2.2.3 Experiment 3: CLDS

Because GCMs have to compute clear-sky radiative fluxes to estimate cloud radiative effects, it is reasonable, though not necessary, to perform a full clear-sky calculation and devote all of McICA's samples to the cloudy (variable) portion of a domain. Thus, by demanding that randomly-generated subcolumns contain cloud, total flux is

$$\langle F \rangle = (1 - A_c) \sum_{k=1}^{K} F(\alpha_{clr}, k) + A_c \sum_{k=1}^{K} F(\alpha_{cld,k}, k) \tag{4}$$

where α_{clr} represents *the* clear-sky subcolumn, $\alpha_{cld,k}$ represents one of K cloudy subcolumns, and A_c is vertically-projected cloud fraction. A_c can be estimated rapidly and accurately by generating many subcolumns with a stochastic cloud generator that avoids estimation of water contents. Since random sampling is confined to cloudy subcolumns, this experiment is referred to as "CLDS ". Obviously, the amount of noise generated by BASIC is greater than or equal to that produced by CLDS.

2.2.4 Experiment 4: SPEC

An efficient way to reduce McICA noise is to sample additional cloudy subcolumns for spectral intervals that contribute most to McICA's noise. These points are generally those with large cloud radiative effects. As such, this version of McICA defines fluxes as

$$\langle F \rangle = (1 - A_c) \sum_{k=1}^{K} F(\alpha_{clr}, k) + A_c \sum_{k=1}^{K} \left[\frac{1}{N_k} \sum_{i=1}^{N_k} F(\alpha_{cld,i,k}, k) \right] \tag{5}$$

where N_k are the number of samples generated for k, and $\mathcal{N} = \sum_{k=1}^{K} N_k$ is the total number of samples generated. This version of McICA is referred to as "SPEC" because additional samples are assigned to specific spectral intervals (cf. the splitting technique as described in Marchuk et al. 1980). Note that for CLDS, $N_k = 1$ and so $\mathcal{N} = K$. It was recommended that for this model, however, $\mathcal{N} \approx 1.5K$. Räisänen and Barker (2004) provide a means to set $\{N_k\}$ that reduces variance optimally.

2.2.5 Experiment 5: Reference simulations (REF)

Finally, a reference experiment, referred to as "REF", was performed, by most GCMs, and characterized by very weak noise. The simplest and most economical way to do this is to use the SPEC model with large $\mathcal{N}$. The GFDL GCM uses a very small number spectral points and therefore its REF experiment was the, less economical, ICA using K subcolumns (see Pincus et al. 2006). Nevertheless, noise associated with REF is much smaller than 1COL's and notably less than SPEC's.

3 Description of GCMs

Tables 1 and 2 summarize characteristics of the GCMs that participated in the intercomparison. CMC and GFDL are finite volume models; the other four are spectral models. Horizontal resolutions varied from ∼100 km to ∼250 km, and number of vertical layers ranged from 24 to 91. While some subgrid-scale parametrizations are common to more than one GCM (e.g., GEM and CCCma used the same radiation codes), and others use parametrizations with common lineages (e.g., ECMWF and ECHAM5), no two GCMs share the exact same collection of parametrizations.

Morcrette (2000) and Räisänen et al. (2005) showed that changing the radiative timestep Δt_{rad} from 1 h to 3 h can influence a GCM's simulation. With McICA there is the added concern that large Δt_{rad} might allow a GCM to incorporate the effects of radiative anomalies into the overall character of the simulation (Räisänen et al. 2005). For the experiments reported here, the GFDL and GEM models were run with a 3 h and 2 h timestep in addition

to a 1 h timestep. Differences between the runs were very minor, so only results for the shorter timestep are discussed hereinafter.

Lacking rules pertaining to description of unresolved horizontal variations in cloud water and vertical overlap of fractional cloud, groups were left to define them for themselves. While this side-steps the utility of McICA, recall that it is the *spread* in McICA-generated stochastic noise that is important for these experiments; details of unresolved cloud morphology are secondary. As seen later, wide ranges of noise were achieved by all GCMs.

4 Results

Results are presented in two sections. The first summarizes variations in stochastic noise as a function of GCM. The second presents GCM responses as a function of noise.

4.1 Magnitude of McICA noise

To quantify the magnitude of the stochastic noise generated for the five experiments, standard deviations of variables responsible for producing noise were computed for each rendition of McICA by generating subgrid-scale clouds and calling the radiation code 10 times at each radiative time-step for a *single day* (see Fig. 3). The variables are SW and LW radiative flux profiles, total cloud fraction, and cloud liquid and ice water paths (actually, water contents are subject to noise directly).

As an illustrative example, Fig. 4 shows standard deviation of SW radiative flux at the surface as a function of the corresponding mean for the 1COL, BASIC, and CLDS

versions. The magnitude of noise and the rate at which it decreases with increasing samples (left to right across the figure) depends on several factors including number of spectral intervals, diurnal cycle of cloud properties, frequency distribution of cloud fraction profile, and assumptions about unresolved clouds. This plot shows the abundance of noise associated with 1COL as well as the dramatic, and ubiquitous, reduction of noise when going from 1COL to BASIC. The only GCM to show a sizable reduction in noise when going from BASIC to CLDS, where the total number of samples remained the same, is the CCCma GCM. The most likely reason for this has to do with the distribution of total cloud fraction; McICA errors maximize at intermediate cloud fractions and vanish at clear-sky and almost vanish at overcast. As Fig. 5 shows, the CCCma GCM has the fewest near-overcast and cloudless cases and a large fraction of total cloud fractions near 0.25. The other GCMs have relatively few intermediate total cloud fractions; especially ECHAM5 which produces numerous near-clear and overcast events. Note that a GCM that produces *only* clear-skies and overcasts will realize minimal variance reduction when going from BASIC to CLDS. This situation should become increasingly prevalent as $\Delta x_{\mathrm{GCM}} \rightarrow 0$.

From Fig. 4 alone one can predict, with reasonable confidence, that most GCMs have little to gain from CLDS, let alone the more elaborate SPEC. Nevertheless, as argued by Räisänen and Barker (2004), all GCMs compute clear-sky fluxes for diagnostic reasons, so there is some motivation to employ CLDS and devote all available stochastic samples to the cloudy, variance-generating, portion of a column.

4.2 Impacts on GCM Simulations

While numerous fields were saved from the simulations, so few exhibited significant differences that presentation of results focuses on low cloud fraction and 2 m air temperature; the variables that showed the greatest sensitivities to noise. Results are presented in two subsections: one focusing on fractional areas of the globe that exhibit statistically significant changes due to noise; and the other on time series analysis.

4.2.1 Fractional areas of statistically significant differences

A convenient way to summarize the kind of results obtained here is the paired-difference version of Student's t-test (e.g., von Storch and Zwiers 1999). This is because ensemble members in one experiment have the same initial conditions as those in another experiment. Hence, the experiments are not fully independent of each other. If two experiments, each with N ensemble members, are being compared and $\mathbf{x}_n$ and $\mathbf{y}_n$ are the nth member of their respective ensembles, define $\mathbf{d}_n = \mathbf{x}_n - \mathbf{y}_n$. The null hypothesis to be tested is therefore H_0: $\mu_{\mathbf{xy}} = 0$, where $\mu_{\mathbf{xy}}$ is mean of the population of differences $\mathbf{d}$ from which the sample, of size N, was drawn. From sampling theory, the optimal test statistic is

$$t = \frac{\widehat{\mu}_{\mathbf{xy}}}{S_{\mathbf{xy}}/\sqrt{N}}, \tag{6}$$

where $\widehat{\mu}_{\mathbf{xy}}$ is sample mean difference, and $S_{\mathbf{xy}}$ is corresponding unbiased sample variance. Assuming that the sample differences follow Student's distribution, t is checked to see if it lies beyond a specified value, the significance level, in the tail of the distribution. This is

done by checking if

$$\frac{1}{\nu^{\frac{1}{2}} B\left(\frac{1}{2}, \frac{\nu}{2}\right)} \int_{-t}^{t} \left(1 + \frac{x^2}{\nu}\right)^{-\frac{\nu+1}{2}} dx > t_{\text{crit}}, \tag{7}$$

where $\nu = N - 1$, $B\left(\frac{1}{2}, \frac{\nu}{2}\right)$ is the beta function, and $t_{\text{crit}} = 1 - \alpha$ where α is the level of significance one is testing for. If (7) is true, the sampled difference is considered to be statistically significant. Throughout this study, $\alpha = 0.05$ implying that all reported tests are at the 95% confidence level. Note that if M samples are drawn at random from a population, and sample pairs are tested via (6) and (7), then on average, αM of them will exhibit statistically significant differences. Reported here are fractional areas of *regions* with GCM cells that exhibit statistically significant differences. The *regions* are typically zonal bands and the entire Earth.

Räisänen et al. (2005) showed that for CAM1.8, low cloud fraction exhibited the greatest sensitivity to McICA noise. Low cloud is defined as cloud below 680 hPa. Figure 6 shows Hovmöller-like diagrams of the fractional area of zonal-bands with statistically significant differences in low cloud fraction for four renditions of McICA relative to REF. The striking aspect of this set of plots is that each model responds differently to McICA noise, though all but some of the 1COL versions display statistically insignificant ramifications of noise. For instance, CCCma and ECHAM5 show almost no dependence on noise level while CAM3 and GFDL experience dramatically reduced sensitivities to noise going from 1COL to BASIC. The two highest resolution models, GEM and ECMWF forecast models, show only a slight dependence on noise level, but, despite being very different models, they share some common features. Namely, remarkably few significant responses in the subtropical high regions with persistent, though minor, differences throughout the tropics. Presumably differences in the

tropics stem from local processes responding very quickly to noise but of such limited strength that their influences are not felt very far outside the cell they were initiated in.

Several models, ECMWF, ECHAM5, GEM, and GFDL, show similar patterns for the mid- and high-latitudes: a rather sudden transition, at roughly 8 days into the simulations, from areas of difference slowly increasing with time to being independent of time. Nevertheless, most latitudes have areas of significant difference of approximately 5% so these appear to be fluctuations due simply to sampling from the same population with little, or nothing, to do with response to noise.

The results just shown are applicable to 2 h instantaneous samples. Figure 7 shows global maps of the location of significant differences in low cloud fraction averaged over the 14th day of the BASIC simulations. In general, the fractional areas showing significant differences relative to REF are much smaller than at the 2 hourly zonal level; the largest area is a meager 3.6% for the CCCma model. Moreover, one is hard-pressed to discern any pattern in any of these plots. This is another positive feature for it suggests that the effects of noise have not been incorporated and transferred up-scale to affect change on regional scales.

Figure 8 shows time series of fractional areas of the globe that exhibit statistically significant noise-induced responses on 2m air temperature as functions of time. As with low cloud, each model displays a unique response to noise. Most models and renditions of McICA begin the simulation looking as though they were drawn from the same population as REF. The 1COL versions of CAM3 and GEM show slight impacts of noise, while the corresponding versions of CCCma and GFDL appear to be heading toward acceptance of H_0 by day-14. Consistent with Räisänen's et al. (2005) analyses, all other cases are statistically indistin-

guishable from REF.

Precipitation is another crucial climatic variable that one would hope is not influenced by noise. Moreover, precipitation fields differ vastly from cloud fraction and temperature on account of their extreme intermittency. Figure 9 shows Hovmöller-like diagrams of fractional areas of significant difference relative to REF for large-scale precipitation for three GCMs and total precipitation for the remaining three. Only 1COL and BASIC are shown. Plotted along the bottom are time series of corresponding global areas. Most plots and curves demonstrate extremely minor affects due to noise; often even smaller than impacts on 2 m temperature. The exception is ECMWF's run with 1COL which shows a marked response in the tropics. Again, however, it is highly unlike that a modelling group would use 1COL, and the impact is clearly crushed by the noise reduction of BASIC; which is ECMWF's operational configuration (see Morcrette et al. 2008).

As a final means of portraying the ramification, or lack thereof, of McICA noise, Fig. 10 shows fractional areas of the globe showing statistically significant changes to low cloud fraction and 2 m temperature averaged over the 14th day as functions of globally-averaged McICA noise associated with net shortwave flux at the surface. These plots show succinctly that if ever there is an issue with noise, it is bound to the 1COL version of McICA. They also show that the CAM stands the most to gain by going from 1COL to BASIC, while the CCCma stands the most to gain by going from BASIC to CLDS.

4.2.2 Time series analysis

An obvious area to look for rapid development of responses due to high frequency noise generated by McICA is in the magnitude of temporal fluctuations for variables φ with short characteristic response times. Variables in the lower atmosphere or at the surface are good candidates; particularly ones that are influenced directly by McICA-related noise. For a discrete time series spanning a length of time L, fluctuations of φ are assessed via the second-order structure function which is defined as

$$S_2(r) = \left\langle \left[\varphi\left(t+r\right) - \varphi\left(t\right)\right]^2 \right\rangle \tag{8}$$

where t is time and r is a time lag. $S_2(r)$ is related, by the Wiener-Khinchine theorem, to the power spectrum (see Davis and Marshak 2005), and is a very intuitive measure of typical fluctuations over a wide range of time. For ranges of r that behave like

$$S_2(r) \sim r^{\zeta(2)}, \tag{9}$$

$$1 < \beta = \zeta(2) + 1 < 3$$

where β is the spectral exponent of the power spectrum.

The region of central Canada bounded by 55°N to 65°N and 95°W to 105°W has a continental winter climate with surface temperatures that are sensitive to the presence of cloud. Averaging over this relatively large area, which is about 7 times as large as the coarsest GCM grid-spacing, should alleviate differences that might arise due to variable grid-spacings among the GCMs. Figure 11 shows $S_2(r)$ for 2 m air temperatures averaged over this region. Clearly, McICA noise has little impact of fluctuations of surface temperature. The

magnitude of differences as a function of McICA noise shown here echo not only other areas of the globe but also resemble closely other surface variables such as precipitation rate and pressure. Note also that all models agree nicely on the magnitude of $S_2(r)$ and that they all show a well-defined scaling regime between roughly $r = 1$ h to $r = 48$ h with $\zeta(2) \simeq 3/2$ (or $\beta \simeq 5/2$).

The variable whose $S_2(r)$ exhibited by far the largest sensitivity to McICA noise was, again, low cloud fraction. Figure 12 shows $S_2(r)$ for low cloud fraction averaged for the region bounded by 5°S to 5°N and 170°E to 180°E. This region showed particular sensitivity to McICA noise as documented by Räisänen et al.(2005) for CAM1.8. The most striking aspect of this plot is the hyper-sensitivity of the GFDL model (regardless of radiation timestep length) to substantial McICA noise generated by 1COL where fluctuations on short time scales are almost an order of magnitude larger than those for REF and $\zeta(2) \simeq 0$ for all r whereas $\zeta(2) \simeq 1$ for REF for $r \lesssim 24$ h. Evidently, McICA noise has added a large amount of variance directly to low cloud fraction estimates coming straight from the cloud parametrization. For its BASIC simulation, however, fluctuations almost match perfectly REF's for all r.

The plot in Fig. 12 for CAM3 shows that fluctuations in low cloud fraction for $r \lesssim 3$ h increase slightly as McICA noise is added. This is perfectly understandable. For larger r, however, the magnitude of typical fluctuations decrease as noise increases which seems to be counter-intuitive. As a result, going from REF to 1COL $\zeta(2)$ changes from $\sim$7/6 to $\sim$5/6. For the CCCma, ECHAM5, and GEM GCMs the introduction of McICA noise has little affect on $S_2(r)$. For ECMWF, however, the magnitude of $S_2(r)$ is *least* for 1COL for

all r. Again, this seems counter-intuitive for it implies that the addition of McICA noise *suppresses*, albeit slightly, fluctuations of low cloud fractions. To lesser extents, this is also the case for ECMWF's 2 m temperature as well as low cloud fraction for CAM3 and GEM.

Another aspect of Fig. 12 to note, though not related directly to McICA noise, is that while three of the GCMs, CAM3, CCCma, and GEM, exhibit clear diurnal cycles in low cloud fraction for this region with relative maxima in $S_2(r)$ at $r = 12 + 24n$ h and minima at $r = 24(n + 1)$ h, for $n = 0, 1, 2, 3 \ldots$, the other three lack a diurnal signal. Moreover, the magnitude of $S_2(r)$, for any r, is 5 to 10 times larger for the CCCma and GEM models than for the other models. These differences swamp McICA-generated differences.

To further the points just discussed, Fig. 13 shows the global impact of McICA noise on $\zeta(2)$ for the semi-diurnal range (i.e., $r \leqslant 12$ h). Consistent with Fig. 12, CAM shows a ubiquitous reduction in $\zeta(2)$ as noise increases; CCCma, ECHAM5, and GEM show almost no affect; and ECMWF exhibits very little impact as well except a slight, but general, and again counter-intuitive, increase in $\zeta(2)$ going from REF to 1COL. The odd man out is GFDL where it is now clear that the massive reduction in $\zeta(2)$ going from REF to 1COL as seen in Fig. 12 is actually a global phenomenon that is far from fully recovered by BASIC. Interestingly, however, the corresponding impacts of McICA noise on $\zeta(2)$ for total precipitation, large-scale precipitation, and 2 m air temperature were all very minor (and not worth showing). Hence, the large changes to fluctuations in low cloud fraction involved non-precipitating clouds.

5 Conclusions

Broadband radiative fluxes computed by the Monte Carlo Independent Column Approximation (McICA) are demonstrably unbiased with respect to the full ICA. As such, McICA represents somewhat of a dénouement for the genre of GCM radiative transfer algorithms that aspire to reproduce full ICA results. The penalty for eliminating biases, however, is random noise. If it so happens that this random noise, extraneous information injected at the GCM's inner-scale, affects statistically significant impacts on GCM simulations, this could render McICA useless. Thus, this paper summarizes the impact of random noise generated by McICA on a diverse group of GCMs.

With the exception of the excessive random noise associated with the 1COL version of McICA, noise produced by all realizations of McICA, from those most likely to be used in GCMs to those that squelch noise unnecessarily, have no statistically significant affects on short, 14-day, GCM simulations. Even for the 1COL version not all GCMs showed a significant response to noise and those that did were not impacted significantly for all variables. For instance, the CAM3 GCM showed significant impacts for low cloud and 2 m surface temperature due to noise from 1COL, but its large-scale precipitation was influenced only very weakly. For the BASIC and CLDS versions of McICA, no model displayed any significant impacts from noise. This corroborates previous studies by Pincus et al. (2003; 2006), Räisänen et al. (2005), and Morcrette et al. (2008) and suggests strongly that for most applications, McICA-generated noise should be of little or no concern.

There were some peculiar results. For example, the two weather forecast models, which

operated at the highest spatial resolution, actually showed a slight reduction in the magnitude of low cloud fluctuations at most frequencies as McICA noise increased. This seems counter-intuitive; one would expect introduction of high-frequency noise to increase high-frequency fluctuations in most variables. Another GCM showed only an increase in high-frequency low cloud fluctuations when noise increased and reductions for frequencies longer than a day.

The experiments performed and assessed here address only the ramifications of noise on fast to intermediate climatic variables. The underlying assumption was that if these variables were not influenced, it is unlikely that McICA's noise could somehow emerge later on. Of course, given the complexity of modern GCMs the validity of this assumption cannot be taken fully for granted. Tests should be extended to interactive ocean-atmosphere GCMs integrated over substantial stretches of time. Nevertheless, until it is demonstrated that omission of 3D radiative transfer effects in conventional GCMs is detrimental to simulations (i.e., the ICA is an inadequate standard), results presented here suggest that McICA should be sufficient for most applications of conventional GCMs.

Acknowledgements. This study was supported by grants from the US Department of Energy (Atmospheric Radiation Measurement (ARM) grants DE-FG02-05ER63955 and DE-FG02-03ER63561) and the Canadian Foundation for Climate and Atmospheric Sciences. P. Räisänen was funded by the Ministry of Transport and Communications Finland (project number 36937/2004).We should also like to thank M. Lazare and B. Dugas for help with running the CCC and GEM GCMs, respectively.

References

[1] Aires, F., and W. B. Rossow, 2003. Inferring instantaneous, multivariate and nonlinear sensitivities for the analysis of feedback processes in a dynamical system: The Lorenz model case study. *Quart. J. Roy. Meteor. Soc.*, **129**, 239–275.

[2] Barker, H. W., 1992: Solar radiative transfer for clouds possessing isotropic variable extinction coefficient. *Q. J. R. Meteorol. Soc.*, **118**, 1145-1162.

[3] Barker, H. W., 1996: A parameterization for computing grid-averaged solar fluxes for inhomogeneous marine boundary layer clouds. Part I: Methodology and homogeneous biases. *J. Atmos. Sci.*, **53**, 2289-2303.

[4] Barker, H. W., G. L. Stephens, and Q. Fu, 1999: The sensitivity of domain-averaged solar fluxes to assumptions about cloud geometry. *Quart. J. Roy. Meteor. Soc.*, **125**, 2127–2152.

[5] Barker, H. W., R. Pincus, and J.-J Morcrette, 2002: The Monte Carlo Independent Column Approximation: Application within Large-Scale Models. In proceedings of the *GCSS-ARM Workshop on the Representation of Cloud Systems in Large-Scale Models*, May 2002, Kananaskis, AB, Canada. Available at: http://www.met.utah.edu/skrueger/gcss-2002/Extended-Abstracts.pdf.

[6] Barker, H. W. and 31 others, 2003: Assessing 1D Atmospheric Solar Radiative Transfer Models: Interpretation and Handling of Unresolved Clouds. *J. Climate*, **16**, 2676–2699.

[7] Cahalan, R. F., W. Ridgway, W. J. Wiscombe, S. Gollmer, and Harshvardhan, 1994: Independent Pixel and Monte Carlo Estimates of Stratocumulus Albedo. *J. Atmos. Sci.*, **51**, 3776–3790.

[8] Cairns, B., A. A. Lacis, and B. E. Carlson, 2000: Absorption within Inhomogeneous Clouds and Its Parameterization in General Circulation Models. *J. Atmos. Sci.*, **57**, 700–714.

[9] Cole, J. N. S., H. W. Barker, W. O'Hirok, E. E. Clothiaux, M. F. Khairoutdinov, and D. A. Randall, 2005: Atmospheric radiative transfer through global arrays of 2D clouds. *Geophys. Res. Lett.,* **32**, L19817, doi: 10.1029/2005GL023329.

[10] Cole, J. N. S., H. W. Barker, D. A. Randall, M. F. Khairoutdinov, and E. E. Clothiaux, 2005b: Global consequences of interactions between clouds and radiation at scales unresolved by global climate models. *Geophys. Res. Lett.*, **32**, L06703, doi:10.1029/2004GL020945.

[11] Collins, W. D., 2001: Parameterization of generalized cloud overlap for radiative calculations in general circulation models. *J. Atmos. Sci.*, **58**, 3224-3242.

[12] Davis, A., P. Gabriel, S. Lovejoy, D. Schertzer, and G. Austin, 1990: Discrete angle radiative transfer - Part III: Numerical results and applications. *J. Geophys. Res.*, **95,** 11,729-11,742.

[13] Fu, Q. and K.-N. Liou, 1992: On the correlated k-distribution method for radiative transfer in inhomogeneous atmospheres. *J. Atmos. Sci.*, **49**, 2139-2156.

[14] Geleyn, J.-F. and Hollingsworth, 1979: An economical analytical method for the computation of the interaction between scattering and line absorption of radiation. *Cont. Atmos. Phys.*, **52**, 1-16.

[15] Intergovernmental Panel on Climate Change (IPCC), 2007: Working Group I Report (WGI): Climate Change 2007: The Physical Science Basis. Available at http://ipcc-wg1.ucar.edu/wg1/wg1-report.html.

[16] Marchuk, G. I., G. A. Mikhailov, M. A. Nazaraliev, R. A. Darbinjan, B. A. Kargin, and B. S. Elepov, 1980: *Monte Carlo methods in atmospheric optics*. Ser. Opt. Sci., **12**, Springer-Verlag, 208pp.

[17] Marshak, A. and A. B. Davis, 2005: Scale-by-scale analysis and fractal cloud models. In *3D Radiative Transfer in Cloudy Atmospheres*, A. Marshak and A. B. Davis, Eds., Springer, Heidelberg, 686 pp.

[18] Meador, W. E. and W. R. Weaver, 1980: Two-stream approximations to radiative transfer in planetary atmospheres: A unified description of existing methods and a new improvement. *J. Atmos. Sci.*, **37**, 630-643.

[19] Morcrette, J.-J., and Y. Fouquart, 1986: The overlapping of cloud layers in shortwave radiation parameterizations, *J. Atmos. Sci.*, **43**, 321-328.

[20] Morcrette, J.-J., 2000: On the effects of the temporal and spatial sampling of radiation fields on the ECMWF forecasts and analyses. *Mon. Weath. Rev.*, **128**, 876–887.

[21] Morcrette, J.-J., H. W. Barker, J. N. S. Cole, M. J. Iacono, and R. Pincus, 2008: Impact of the new radiation package, McRAD, in the ECMWF integrated forecast system. In press: *Mon. Wea. Rev.*

[22] Oreopoulos, L., and H. W. Barker, 1999: Accounting for subgrid-scale cloud variability in a multi-layer, 1D solar radiative transfer algorithm. *Q. J. R. Meteorol. Soc.,* **125**, 301-330.

[23] Phillips, T. J., G. L. Potter, D. L. Williamson, R. T. Cederwall,

[24] J. S. Boyle, M. Fiorino, J. J. Hnilo, J. G. Olson, S. Xie, and J. J. Yio, 2004: The CCPP-ARM Parameterization Testbed (CAPT): Evaluating climate models in a weather forecasting framework. 15th Symposium on Global Change and Climate Variations. See http://ams.confex.com/ams/pdfpapers/73412.pdf.

[25] Pincus, R., H. W. Barker, and J.-J. Morcrette, 2003: A fast, flexible, approximate technique of computing radiative transfer for inhomogeneous clouds. *J. Geophys. Res.*, **108**, 4376, doi:10.1029/2002JD003322.

[26] Pincus, R., R. Hemler, and S. A. Klein, 2006: Using stochastically generated subcolumns to represent cloud structure in a large-scale model. *Mon. Wea. Rev.*, **134**, 3644-3656.

[27] Randall, D., M. Khairoutdinov, A. Arakawa and W. Grabowski, 2003: Breaking the cloud parameterization deadlock. *Bull. Am. Met. Soc.*, **84**, 1547–1564.

[28] Räisänen, P., H. W. Barker, M. Khairoutdinov, J. Li, and D. A. Randall, 2004: Stochastic generation of subgrid-scale cloudy columns for large-scale models. *Quart. J. Roy. Meteor. Soc.*, **130**, 2047–2067.

[29] Räisänen, P. and H. W. Barker, 2004: Evaluation and optimization of sampling errors for the Monte Carlo independent column approximation. *Quart. J. Roy. Meteorol. Soc.*, **130**, 2069-2086.

[30] Räisänen, P., H. W. Barker and J. Cole, 2005: The Monte Carlo Independent Column Approximation's Conditional Random Noise: Impact on Simulated Climate. *J. Climate*, **17**, 4715-4730.

[31] Stephens, G. L., 1988: Radiative transfer through arbitrary shaped optical media: Part II: Group theory and simple closures. *J. Atmos. Sci.*, **45**, 1837-1848.

[32] Stephens, G. L., P. M. Gabriel, and S.-C. Tsay, 1991: Statistical radiative transfer in one-dimensional media and its application to the terrestrial atmosphere. *Trans. Theory Stat. Phys.*, **20**, 139-175.

[33] Stephens, G. L., 2005: Cloud feedbacks in the climate system: A critical review. *J. Climate*, **18**, 237–273.

[34] Stubenrauch, C. J., A. D. Del Genio, and W. B. Rossow, 1997: Implementation of subgrid cloud vertical structure inside a GCM and its effect on the radiation budget. *J. Climate*, **10**, 273–287.

[35] Tompkins, A. M., 2002: A prognostic parameterization for the subgrid-scale variability of water vapor and clouds in large-scale models and its use to diagnose cloud cover. *J. Atmos. Sci.*, **59**, 1917–1942

[36] Tian, L. and J. A. Curry, 1989: Cloud overlap statistics. *J. Geophys. Res.*, **94,** 9925-9935.

[37] von Storch, H. and F. W. Zwiers, 1999: *Statistical Analysis in Climate Research.* Cambridge University Press, Cambridge, 484pp.

[38] Wiscombe, W. J., 1977: The delta-Eddington approximation for a vertically inhomogeneous atmosphere. NCAR Tech. Note, TN-121+STR, 66 pp.

Table 1. Summary of the characteristics of participating GCMs.

institute	model	resolution	dynamic time step (min.)	save interval (hr.)
EC-CMC	GEM	1.5°×1.5°; L60	30	2
EC-CCCma	CCCma	T47; L35	20	2
FMI	ECHAM5-FMI	T42; L31	20	2
ECMWF	ECMWF	T_L159; L91	60	2
GFDL	GFDL-AM2	2°×2.5°; L24	60	1 and 3
PSU	CAM3_PSU	T42; L26	60	1

Table 2. Summary of the characteristics of GCM radiative transfer models.

model	quadrature pts (SW/LW)	radiation time-step
GEM	35/46	1 h
CCCma	35/46	1 h
ECHAM5-FMI	4/140	1 h
ECMWF	112/140	1 h
GFDL	18/7	1 h
CAM3_PSU	55/67	1 h

Figure captions

Fig. 1. Left plot shows diurnal-mean solar irradiance at the top-of-atmosphere (TOA) as a function of time and latitude. Right plot shows corresponding standard deviation of solar irradiance at the TOA due simply to Earth's rotation. Corresponding values for net surface irradiance are about half those shown here. Light and dark shaded regions denote perpetual Sun-up and Sun-down periods, respectively.

Fig. 2. Schematic diagram showing production of ensembles of 14-day simulations. All GCMs produced 10-member ensembles (i.e., $M = 10$) though not all performed all 5 ensembles which are denoted here as: 1COL; BASIC; CLD; SPEC; and REF.

Fig. 3. Schematic diagram showing production of noise estimates for various renditions of McICA (denoted here as: 1COL; BASIC; CLD; SPEC; and REF).

Fig. 4. Standard deviation σ of surface solar irradiance as a function of mean solar irradiance μ for three versions of McICA (1COL, BASIC, and CLD) for the six GCMs considered in this study. Colours indicate the natural logarithm of the number of samples in each bin (of which there are 15x15).

Fig. 5. Area-weighted relative frequencies of total cloud fraction for the entire Earth for the six GCMs used in this study. $f_{0.05}$ and $f_{0.95}$ refer to the fractional areas with total cloud fractions less than 0.05 and greater than 0.95.

Fig. 6. Hovmöller-like diagrams of fractional areas of zonal bands exhibiting statistically significant differences, at the 95% confidence level, in low cloud fraction for the various renditions of McICA relative to their respective reference (REF) simulations. McICA noise decreases from left to right. Note that if samples were drawn only from the REF simulation (i.e., the experimental samples were unambiguously pulled from the control population), plots would be characterized by white noise, resembling "snow" on a TV screen, with means of 0.05.

Fig. 7. Global plots showing statistically significant differences between mean low cloud fractions on the 14th day of the simulations for the BASIC rendition of McICA relative to the corresponding REF control. Light blue and red correspond to under- and over-estimations by BASIC that are significant at the 95% confidence level. Likewise, dark blue and red signify the same but at the 99% confidence level. The GCM is indicated in the title along with the fractional area of the globe having statistically significant differences at the 95% confidence level.

Fig. 8. Fractional areas of the globe exhibiting statistically significant 2 m air temperature differences, at the 95% confidence level, relative to the REF control as functions of time for all experiments performed by all GCMs. Had the experiments been drawn from the control population, lines would have been noisy with means very close to 0.05; as most of the curves are beyond about the 10th day.

Fig. 9. Along the top are two rows of Hovmöller-like diagrams of fractional areas of zonal bands exhibiting statistically significant differences, at the 95% confidence level, in precipitation for the 1COL and BASIC renditions of McICA relative to their respective reference (REF) simulations. Had samples been drawn only from the REF simulation, plots would have been characterized by white noise with a mean of 0.05 (corresponding to the 95% confidence level). The lower row of line plots show corresponding fractional areas of the globe exhibiting statistically significant precipitation differences, at the 95% confidence level, relative to the REF control as functions of time. Had the experiments been drawn from the control population, lines would have been noisy with means very close to 0.05.

Fig. 10. Plot on the left shows fractional areas of the globe exhibiting statistically significant differences, at the 95% confidence level, as a function of McICA noise (i.e., standard deviation) associated with net shortwave surface irradiance. Plot on the left is the same except it applies to 2 m air temperature. 1COL results are on the right-side of the plots.

Fig. 11. Second-order structure functions for 2 m air temperature averaged over the region indicated in the title as functions of lag time. Results are shown for three versions of McICA for each GCM. All analyses were for data with 2 h timesteps save for the CAM3 GCM which had a 1 h step. Grey line is for reference and highlights the consistency among GCMs and McICA noise levels.

Fig. 12. Second-order structure functions for low cloud fraction averaged over the region indicated in the title as functions of lag time. Results are shown for three versions of McICA for each GCM. All time series used data with 2 h timestep save for the CAM3 GCM which had a 1 h step. Vertical lines are for reference and indicate periods of 12 and 24 h.

Fig. 13. Global plots of the scaling exponent $\zeta(2)$ in (9) for low cloud fraction for three versions of McICA. These quantities correspond to the scaling regions shown in Fig. 12 for $r \leqslant 12$ h.

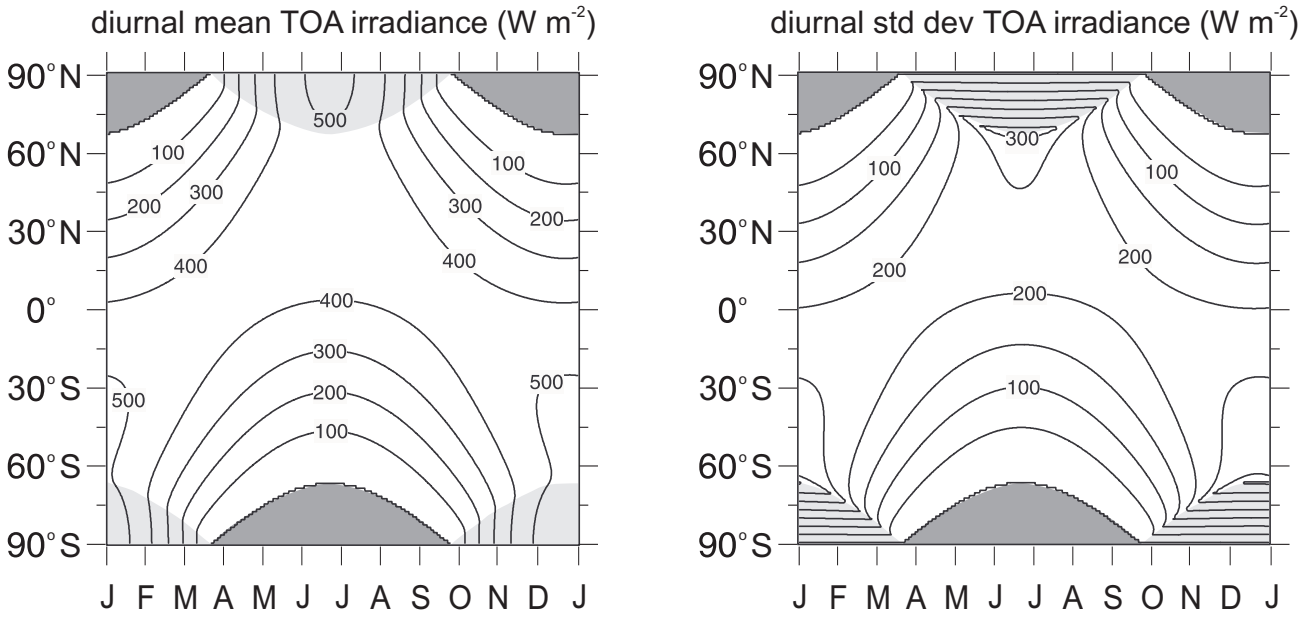

Fig. 1. Left plot shows diurnal-mean solar irradiance at the top-of-atmosphere (TOA) as a function of time and latitude. Right plot shows corresponding standard deviation of solar irradiance at the TOA due simply to Earth's rotation. Corresponding values for net surface irradiance are about half those shown here. Light and dark shaded regions denote perpetual Sun-up and Sun-down periods, respectively.

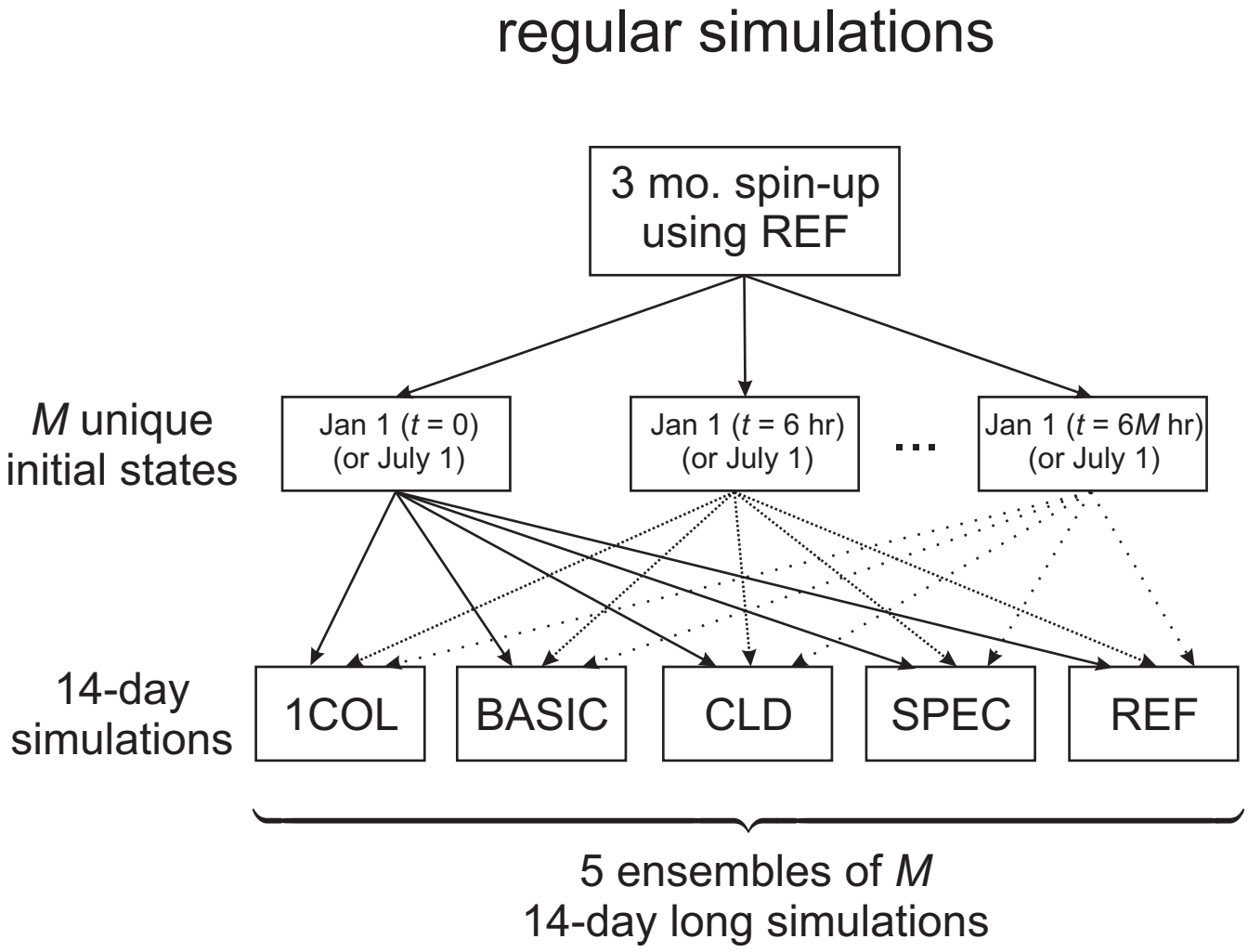

Fig. 2. Schematic diagram showing production of ensembles of 14-day simulations. All GCMs produced 10-member ensembles (i.e., $M = 10$) though not all performed all 5 ensembles which are denoted here as: 1COL; BASIC; CLD; SPEC; and REF.

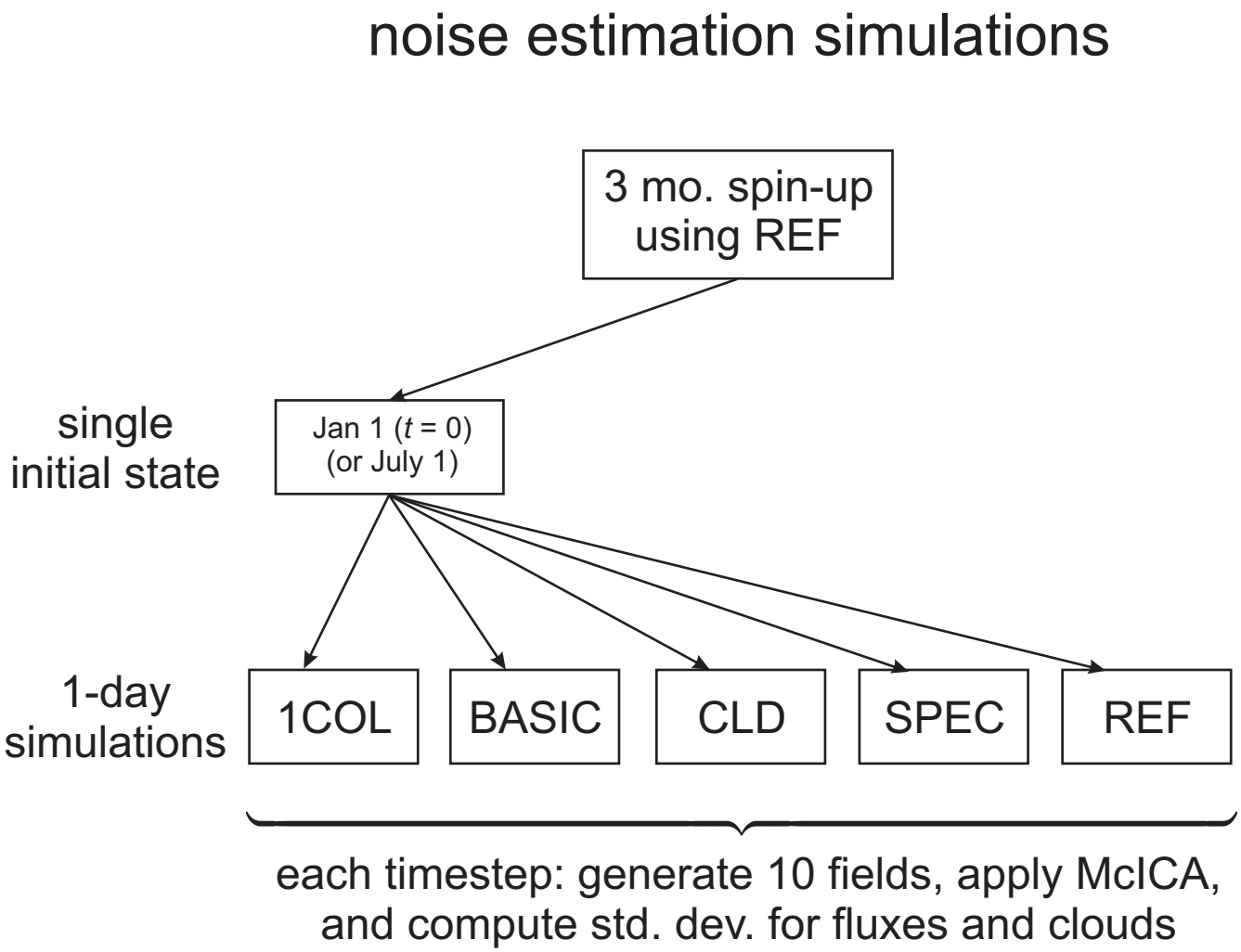

Fig. 3. Schematic diagram showing production of noise estimates for various renditions of McICA (denoted here as: 1COL; BASIC; CLD; SPEC; and REF).

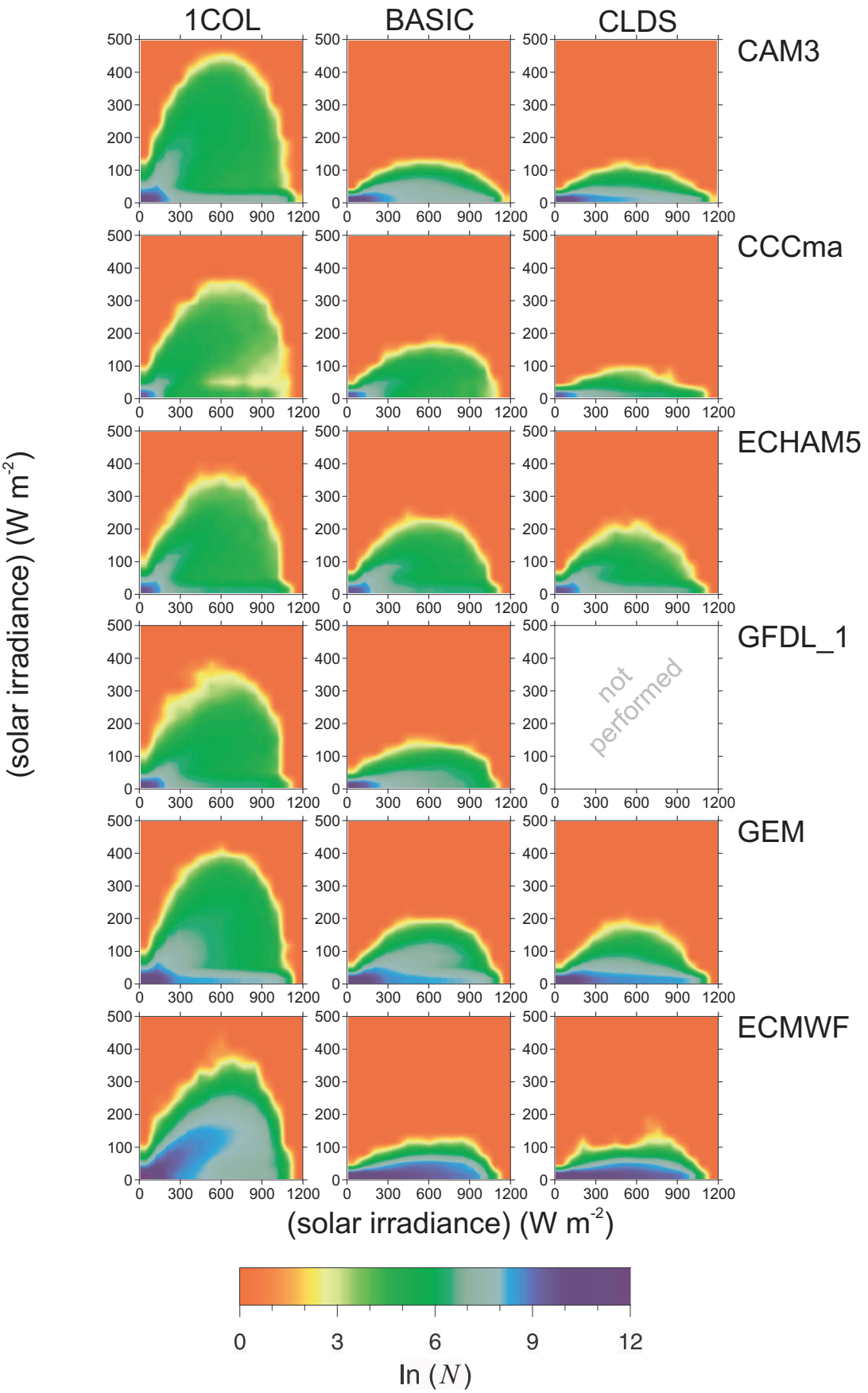

Fig. 4. Standard deviation σ of surface solar irradiance as a function of mean solar irradiance μ for three versions of McICA (1COL, BASIC, and CLD) for the six GCMs considered in this study. Colours indicate the natural logarithm of the number of samples in each bin (of which there are 15x15).

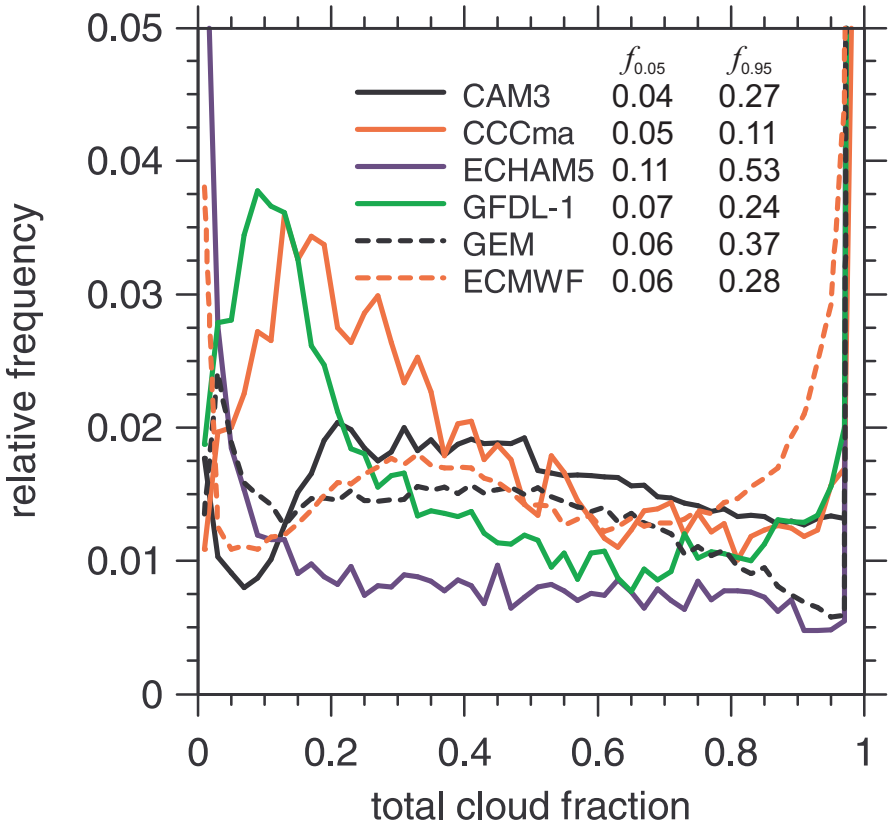

Fig. 5. Area-weighted relative frequencies of total cloud fraction for the entire Earth for the six GCMs used in this study. $f_{0.05}$ and $f_{0.95}$ refer to the fractional areas with total cloud fractions less than 0.05 and greater than 0.95.

low cloud fraction

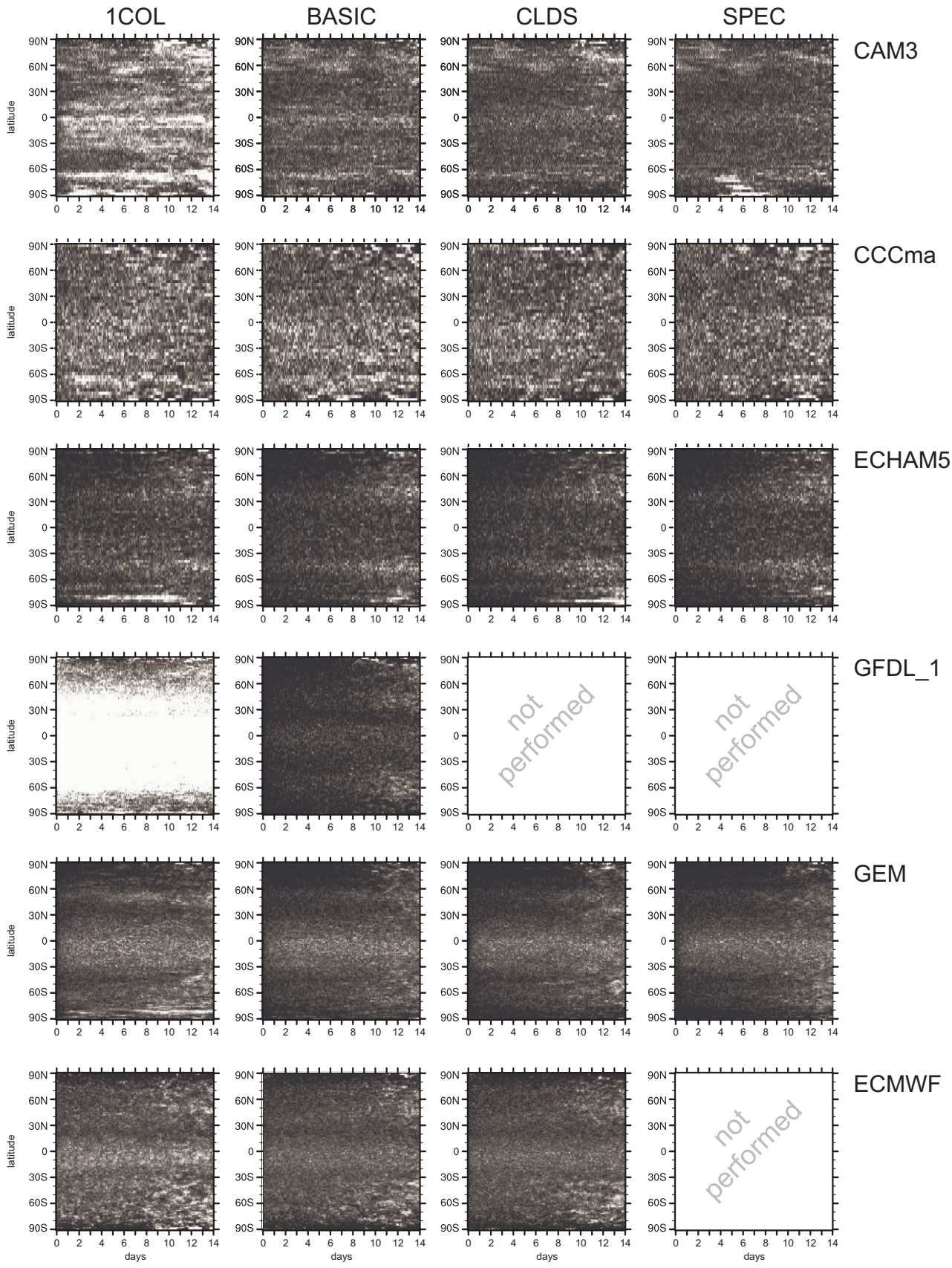

Fig. 6. Hovmöller-like diagrams of fractional areas of zonal bands exhibiting statistically significant differences, at the 95% confidence level, in low cloud fraction for the various renditions of McICA relative to their respective reference (REF) simulations. McICA noise decreases from left to right. Note that if samples were drawn only from the REF simulation (i.e., the experimental samples were unambiguously pulled from the control population), plots would be characterized by white noise, resembling "snow" on a TV screen, with means of 0.05.

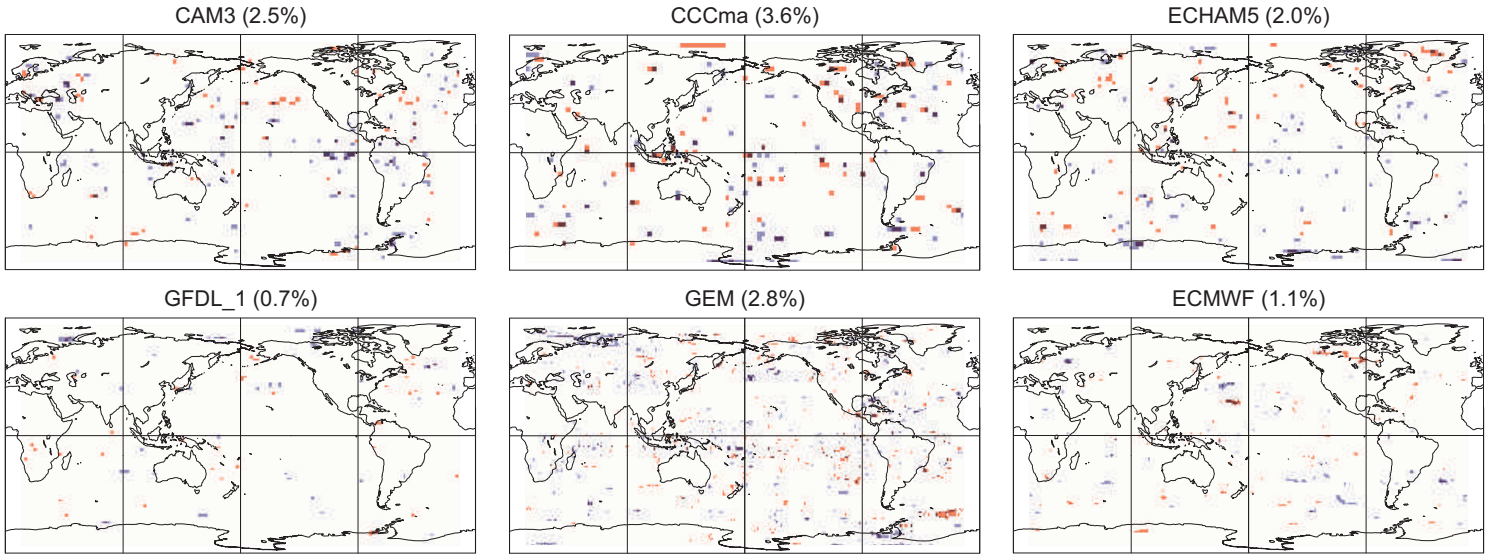

Fig. 7. Global plots showing statistically significant differences between mean low cloud fractions on the 14th day of the simulations for the BASIC rendition of McICA relative to the corresponding REF control. Light blue and red correspond to under- and over-estimations by BASIC that are significant at the 95% confidence level. Likewise, dark blue and red signify the same but at the 99% confidence level. The GCM is indicated in the title along with the fractional area of the globe having statistically significant differences at the 95% confidence level.

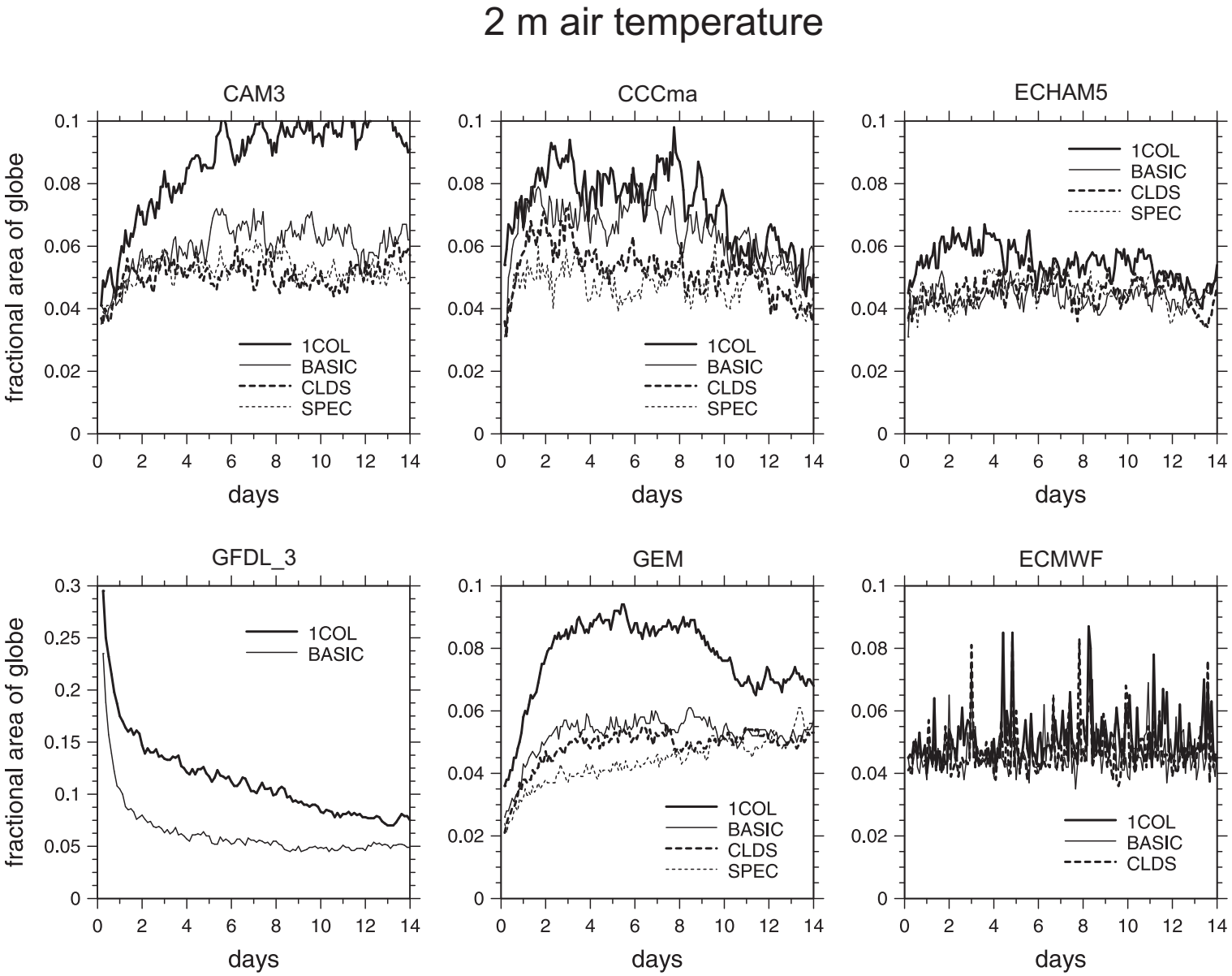

Fig. 8. Fractional areas of the globe exhibiting statistically significant 2 m air temperature differences, at the 95% confidence level, relative to the REF control as functions of time for all experiments performed by all GCMs. Had the experiments been drawn from the control population, lines would have been noisy with means very close to 0.05; as most of the curves are beyond about the 10th day.

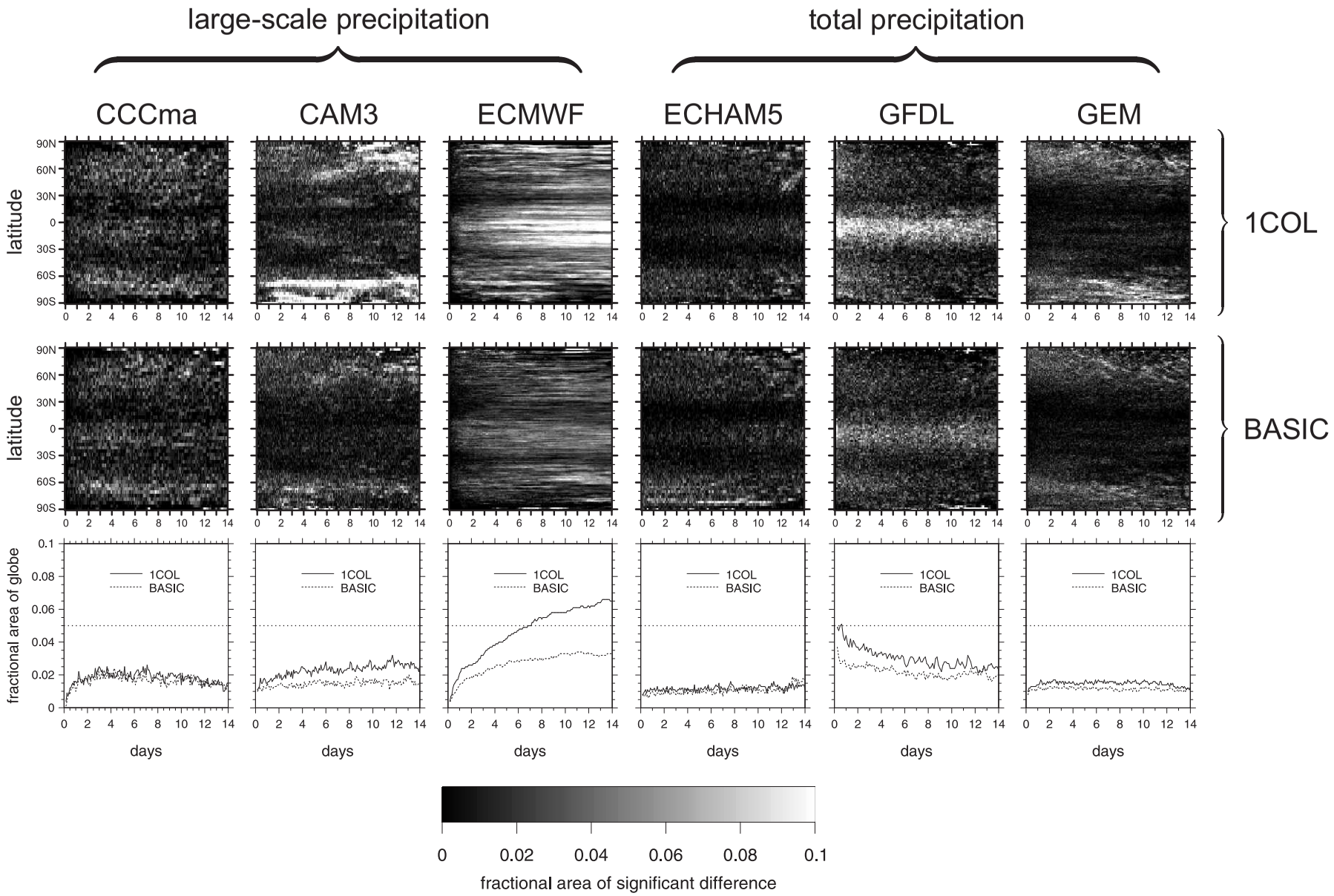

Fig. 9. Along the top are two rows of Hovmöller-like diagrams of fractional areas of zonal bands exhibiting statistically significant differences, at the 95% confidence level, in precipitation for the 1COL and BASIC renditions of McICA relative to their respective reference (REF) simulations. Had samples been drawn only from the REF simulation, plots would have been characterized by white noise with a mean of 0.05. The lower row of line plots show corresponding fractional areas of the globe exhibiting statistically significant precipitation differences, at the 95% confidence level, relative to the REF control as functions of time. Had the experiments been drawn from the control population, lines would have been noisy with means very close to 0.05.

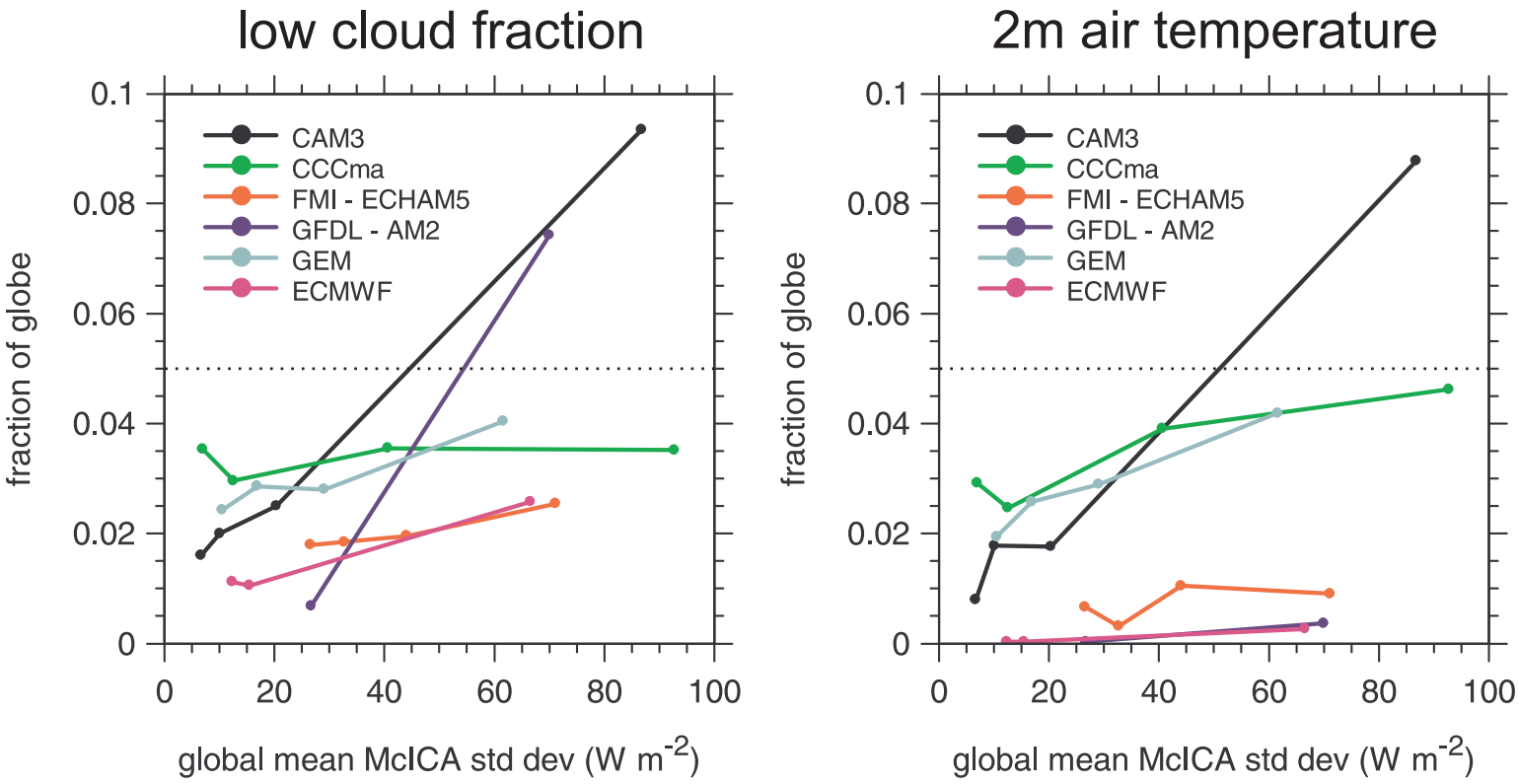

Fig. 10. Plot on the left shows fractional areas of the globe exhibiting statistically significant differences, at the 95% confidence level, as a function of McICA noise (i.e., standard deviation) associated with net shortwave surface irradiance. Plot on the left is the same except it applies to 2 m air temperature.

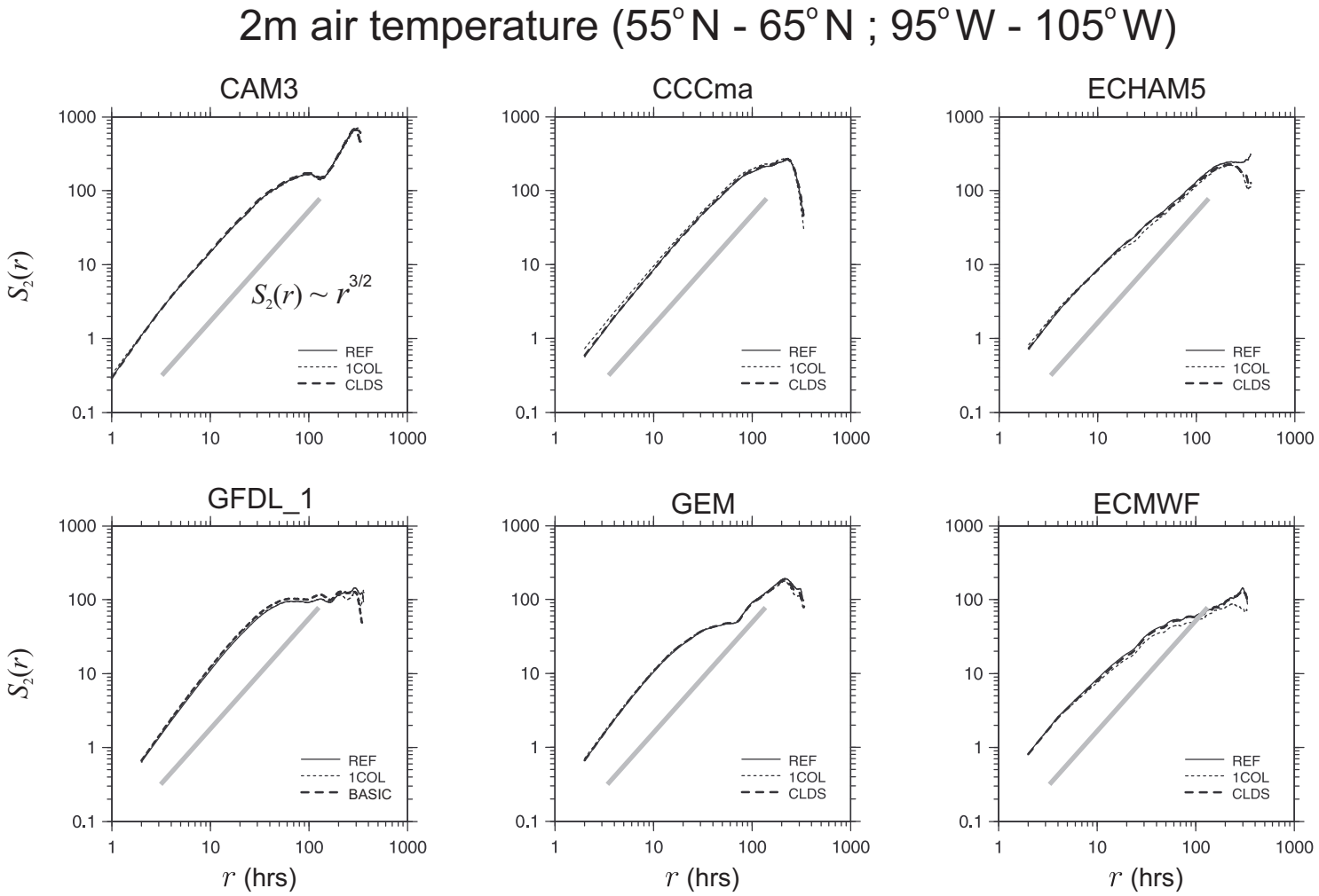

Fig. 11. Second-order structure functions for 2 m air temperature averaged over the region indicated in the title as functions of lag time. Results are shown for three versions of McICA for each GCM. All analyses were for data with 2 h timesteps save for the CAM3 GCM which had a 1 h step. Grey line is for reference and highlights the consistency among GCMs and McICA noise levels.

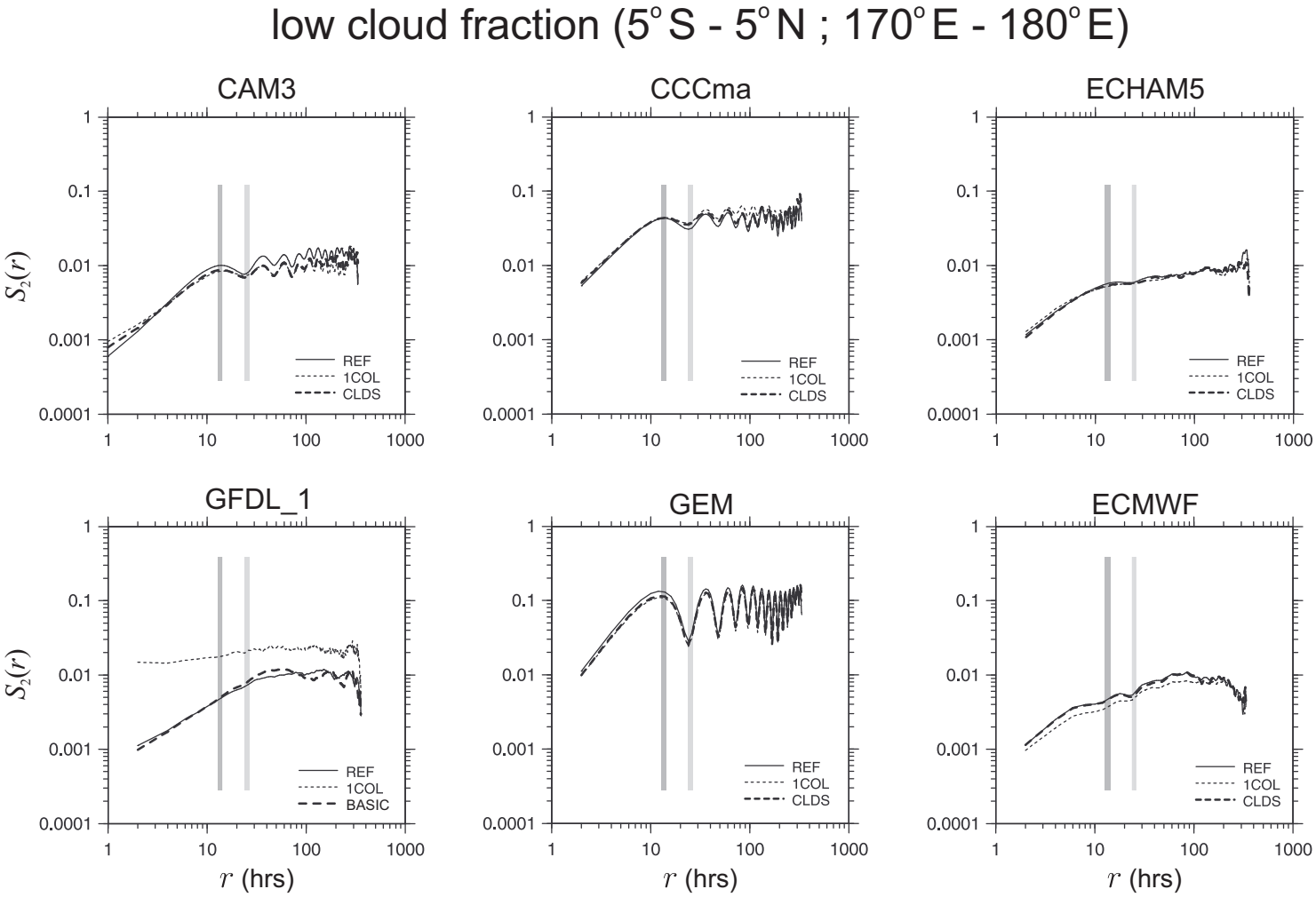

Fig. 12. Second-order structure functions for low cloud fraction averaged over the region indicated in the title as functions of lag time. Results are shown for three versions of McICA for each GCM. All time series used data with 2 h timestep save for the CAM3 GCM which had a 1 h step. Vertical lines are for reference and indicate periods of 12 and 24 h.

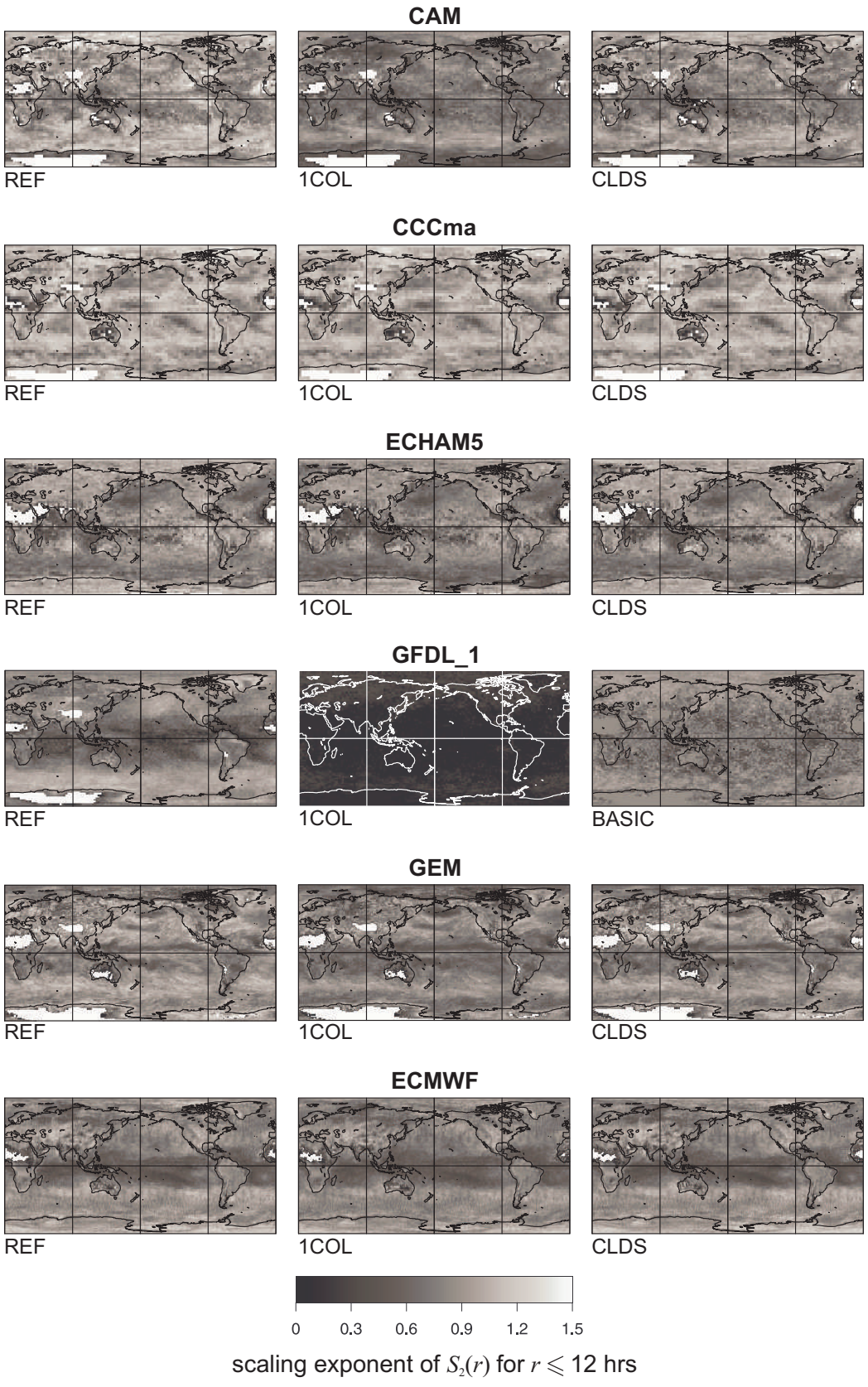

Fig. 13. Global plots of the scaling exponent $\zeta(2)$ in (8) for low cloud fraction for three versions of McICA. These quantities correspond to the scaling regions shown in Fig. 12 for $r \leqslant 12$ h.